# Structural instabilities of excited phases

P. J. Craievich and J. M. Sanchez
*Center for Materials Science and Engineering, The University of Texas at Austin, Austin, Texas 78712*

R. E. Watson and M. Weinert
*Department of Physics, Brookhaven National Laboratory, Upton, New York 11973–5000*

(Received 29 July 1996)

The structural stability of various elemental metals (Ti, Sc, Al, Mo, and Nb), ordered compounds (PtTi and PtV), and disordered Ni-Cr alloys along distortion paths linking high-symmetry structures are investigated. A number of high-symmetry nonequilibrium structures are found to be mechanically unstable for these deformation paths, even for structures that occur at high temperature. For Ti, the electronic entropy is found to stabilize of the bcc phase at high temperatures, but without vibrational effects the hcp↔bcc transition would occur at much higher temperatures than observed. To treat disordered alloys along the Bain distortion path, the cluster expansion method is applied to the body-centered-tetragonal lattice, with particular choices of clusters in order to guarantee that the effective cluster interactions comply with the symmetry conditions of the cubic lattices. For disordered Ni-Cr alloys, the range of composition where the bcc and fcc phases are mechanically stable is determined. [S0163-1829(97)00102-1]

## I. INTRODUCTION

The energies and entropies of both equilibrium and nonequilibrium phases are important to the phase diagram behavior of metals and alloys. Besides the issue of what are the low-temperature equilibrium phases, there are cases of structural phase transitions at elevated temperatures. In addition, excited phases of some composition can have consequences for the alloying at another composition. Many such phases can be related to another by lattice distortions: perhaps the most famous example of these is the Bain distortion which takes a bcc lattice into (or from) an fcc lattice via a tetragonal distortion. It has been generally presumed that excited structural phases, particularly if they are observed high-temperature phases, are metastable. Previously we have shown[1,2] that large classes of these phases are, in fact, not metastable but instead are locally unstable, i.e., are unstable to lattice distortions. These instabilities can be seen in a number of previous calculations[3–6] and have implications for phase diagram constructs.[7–9]

The objectives of the present paper are threefold: First, to demonstrate that the mechanical instabilities found previously are, in fact, ubiquitous; secondly, to show that these effects are not limited to ordered systems, but may also occur in disordered alloys; and thirdly, to show that these types of instabilities may be present in systems that are stabilized by entropy at high temperatures. Although these issues related to phase (in)stability seem at first glance independent of each other, they all need to be considered if one is to gain a better understanding of phase diagrams from a microscopic (electronic structure) point of view.

Previously[1] a condition regarding the topology of the energy surface along certain distortions was derived indicating when the energy must be an extremum along the path and examples were given for systems connected by Bain distortions. The present paper will consider several other cases of the Bain distortion and will also inspect deformation paths connecting the bcc↔hcp, AuCd↔CsCl, and AuCd ↔CuAu-I structures. The latter two are appropriate to the Martensitic transformations from the low-temperature AuCd phases of PtTi and PtV, respectively; in one case the high-temperature phase is metastable along the distortion path considered, while the other is locally unstable. In addition, disordered Ni-Cr alloys along the Bain distortion path and the mechanical stability of the cubic alloy phases as a function of composition will also be considered. The Ni-Cr system was chosen since the instability of the Cr fcc phase is severe[1] and Ni-Cr has both a fcc stable (Ni-rich side of the phase diagram) and a bcc stable (Cr-rich) region.[10]

The extremal condition arises when a lattice distortion of some given symmetry, for example tetragonal or orthorhombic, passes through a structure of higher symmetry. If the distortion path is described in terms of a parameter constrained to satisfy certain conditions, the derivative of the energy with respect to the distortion parameter will be, by symmetry, zero valued upon passing through structures of higher symmetry. Thus, the energy will be a minimum, a maximum, or an inflection point for such structures. In the case of the tetragonal Bain distortion path for an elemental solid or a disordered alloy, the condition requires that the energies of the fcc and bcc phases must be extrema. For a binary ordered compound along a distortion path passing through the CsCl and the CuAu-I structures, however, the condition applies to the cubic bcc-like CsCl phase, but not to the fcc-like CuAu-I. Even though the latter is on an fcc lattice, the atomic packing makes the intrinsic symmetry tetragonal and hence the same as the distortion. Of course, there may well be an extremum near the CuAu-I structure, but its $c/a$ value will not be dictated by symmetry. (Experimentally, most compounds that form in the CuAu-I structure have $c/a$ values deviating from the ideal fcc value.) While the Bain distortion is the best known case, distortion paths with symmetry-dictated extrema can be derived for other cases also; for example, the bcc↔hcp path is discussed in Appen-

 

dix A. It is important to note that not all paths connecting two high-symmetry phases will have symmetry-dictated extrema and even small deviations from the path may destroy the extremal properties.

The present investigations use first-principles methods utilizing the local-density approximation (LDA) for exchange and correlation. The utility of this class of calculations for elemental solids and their compounds has been the object of study for some years. As a rule, the observed low-temperature phase has a computed total energy which is stabler than that of other phases at the same composition and, for compounds, more stable than the two-phase mixture of phases at different composition, i.e., the observed phases are correctly predicted. Calculated enthalpies of formation are generally in accord with experiment for those phases for which there are experimental data; even the calculated enthalpies of transformation, e.g., the Ti hcp↔bcc transition, are in agreement although the high-temperature phase is locally unstable. This latter observation would suggest that LDA is as accurate for nonequilibrium as it is for equilibrium phases. There are, however, significant long standing discrepancies between LDA predictions and certain successful constructs of phase diagrams. In particular, in the 1960's Kaufman and Bernstein[7] developed empirical models that are widely used to fit equilibrium phase diagrams of binary and multicomponent systems. In their scheme the energy differences between equilibrium and nonequilibrium structures of the pure elements play a key role. Although there is agreement between the LDA and the empirical modeling in many cases, there have been two important areas of disagreement concerning the structural energy differences. First, the scale of the energy differences between the bcc and the close-packed fcc and hcp phases for metals in the middle of the transition metal row deviate significantly. In a number of cases, these discrepancies are outside the LDA errors encountered when calculated heats of formation or structural energy differences may be compared with experiment. This issue remains unresolved between the two communities of practitioners. Secondly, the empirical construct requires that for the bcc metals of the V and Cr columns of the periodic table, the excited hcp structure be more bound than the fcc. LDA calculations to date have universally placed the fcc lower in energy, although the impact of the $c/a$ ratio on the energies of the hcp lattices was not investigated sufficiently.

The bcc↔hcp distortion path will be considered for Nb and Mo, along with the hcp–fcc energy differences as a function of the hcp $c/a$ ratios. Nb—but *not* Mo (nor Ta and W for which results have been previously obtained[11])—will be seen to have the hcp phase lower in energy, consistent with the demands of Kaufman's empirical construct and contrary to general LDA experience. It should be noted that such phase diagram constructs strongly depend on the nonequilibrium structures being metastable and, as observed above, this is generally not the case. This issue has been discussed recently[1,8,12] and there is a growing consensus that in those cases where the excited phases are locally unstable, the structural energy differences of the empirical constructs are effective rather than true thermodynamic quantities. Finally, the question of the extent to which the electronic entropy may act to stabilize the high-temperature bcc phase of Ti which is locally unstable at zero temperature relative to the low-temperature hcp phase will be considered.

## II. CALCULATIONS

### A. Ordered systems

The calculations for all the systems but Ni-Cr and the results in Appendix B employ the full-potential linearized augmented Slater-type orbital method[13] (FLASTO). In this method, Slater-type orbitals are used to construct wave functions in the interstitial region, augmented by explicit solutions of radial wave equations within nonoverlapping atomic spheres at each atomic site for orbital momenta up to $\ell=8$. Aspherical electron density and potential terms are kept throughout space and the core electrons are treated self-consistently and fully relativistically. Spin-orbit effects were neglected in the self-consistent treatment of the valence shells, although they were turned on in a final iteration in most cases. When dealing with systems involving transition metals, FLASTO may be considered superior to computational schemes neglecting aspherical terms and comparable to or superior to other schemes employed to estimate differences in energies between systems with the exception of the full-potential linearized augmented plane-wave method[14] which utilizes a more complete basis set in the interstitial region. The Hedin-Lundqvist formalism for the local-density exchange and correlation potential was adopted.

Sets of special $k$ points were used and were increased in size until details such as the behavior of the energy in the vicinity of an extremum were accurately established. For example, calculations following a Bain distortion employed sets of 40, 126, 405, and 550 $k$ points and the latter two sets were in agreement for the systems reported here. (This was not the case for Li (Ref. 15) which very likely has the same instability to local distortions as will be seen here). Slater-type orbital basis sets of varying size were employed with the largest involving 2 $s$-, 2 $p$-, 3 $d$-, 1 $f$-, and 1 $g$-like orbital for a transition metal and 2 $s$-, 2 $p$-, a $d$-, and an $f$-like set for Al.

The remaining total-energy calculations used the linearized muffin-tin orbital in the atomic-sphere approximation (LMTO-ASA).[16] This method allows, in a reasonable amount of time, the calculation, of the large number of structures usually required by the cluster expansion method discussed below. The calculations using the LMTO-ASA method were carried out self-consistently, including scalar-relativistic effects, but disregarding magnetic effects. The calculations used a basis set involving $s$, $p$, and $d$ orbitals, and the Barth-Hedin formalism was used for the exchange-correlation potential. The calculations used a number of $k$ points such that the total energy of the structures changed less $\sim 0.1$ mRy/atom. Depending on the number of atoms in the structure's basis, the number of $k$ points in the calculation ranged from 288 to 1000 points in an irreducible wedge of the Brillouin zone. The number of $k$ points were then kept constant for each structure throughout the Bain distortion path.

### B. Cluster expansion

To calculate the energy of the Ni-Cr disordered phase deformed through the Bain distortion path, the cluster expan-

sion method[17,18] was used. In this method, a spinlike occupation number $\sigma_i$ is assigned to each lattice point $i$ in the crystal. The set of $N$ occupation numbers $\vec{\sigma}=\{\sigma_1,\ldots,\sigma_N\}$, where $N$ is the number of sites in the crystal, fully specify the configuration of the system. In the cluster expansion method, the energy (or any function of a configuration $\vec{\sigma}$) is written as a weighted sum of the multisite cluster functions $\Phi_n(\vec{\sigma})$:

$$E(\vec{\sigma})=\sum_n V_n\Phi_n(\vec{\sigma}). \tag{1}$$

The cluster functions form a complete basis in configurational space and the expansion coefficients $V_n$ are called effective clusters interactions (ECI's). In general, the ECI's are of short range, which allows the expansion to be truncated at a reasonably small number of clusters. It may be shown that the ECI's have the symmetry of the lattice. This requirement allows one to group $\Phi_n(\vec{\sigma})$ in sets of equivalent clusters. The average over the set of all clusters functions related by the symmetry of the lattice is called a correlation function, and if multiplied by the degeneracy of the ECI, can be used for the expansion.

Since for the Ni-Cr system we are interested in the Bain deformation path, the body-centered-tetragonal lattice is used for the cluster expansion.[19,20] The ECI's can be determined by matrix inversion or by a least-square fit using the calculated energies of selected structures at various volumes and $c/a$ ratios, and their correlation functions.[21] These ECI's will then have a volume and $c/a$ ratio dependence, and the energy for any ordered or disordered structure in the tetragonal lattice can be calculated. It is noted that at $c/a=1$ and $c/a=\sqrt{2}$ the lattice is cubic so the ECI's at these $c/a$ ratios must have the symmetry of the cubic lattice.

In order to determine the ECI's as a function of $c/a$ ratio, we first consider the points of cubic symmetry of the lattice. At $c/a=1$ and $c/a=\sqrt{2}$ the ECI's were fitted to the calculated formation energies of the ordered structures at a constant volume using a cluster expansion in a cubic lattice. Except for the empty and the point clusters, the clusters used for the expansion in the bcc and fcc lattice are drawn with full line in Fig. 1. The bcc cluster expansion included, in addition to the empty and point clusters, pairs up to the fourth neighbor, three three-body clusters, and two four-body clusters. The fcc cluster expansion included the empty and the point clusters, pairs up to third neighbor, three three-body clusters, and two four-body clusters. In Fig. 1 the lines connecting the bcc and fcc clusters show the relation between the clusters in the two cubic lattices when deformed through a Bain distortion path. As the $c/a$ ratio changes from the points of cubic symmetry, the sets of equivalent clusters may split into two or more sets of clusters in the body-centered-tetragonal (bct) lattice. Note that due to the truncation of the cluster expansion, some of these clusters in the tetragonal lattice do not form a complete set when the $c/a$ ratio reaches the opposite point of cubic symmetry. These incomplete clusters are shown in dashed lines in Fig. 1, and were constrained to be zero so that the truncation in the tetragonal lattice was in agreement with the one adopted in the cubic lattices.

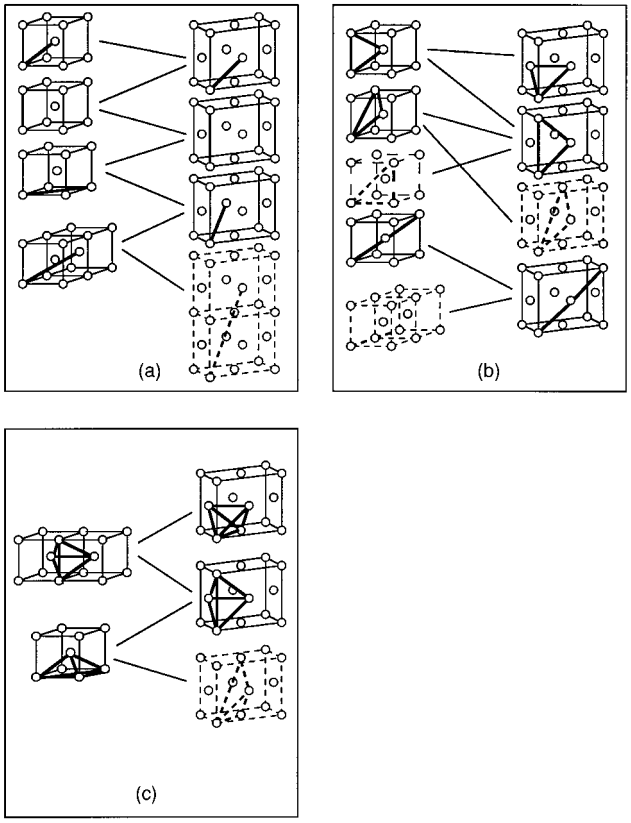


FIG. 1. (a) Pair, (b) three-body, (c) and four-body clusters of lattice points used in the cluster expansion. Clusters drawn with continuous lines are used for the expansions of the cubic lattices; the clusters drawn with broken lines are used for the expansion of the tetragonal lattices but are incomplete at points of cubic symmetry.

To determine the ECI's for $c/a$ ratios other than 1 or $\sqrt{2}$, we chose to fit the expansion parameters by minimizing the error in the energy differences of the structures relative to its energies in the cubic lattice. The formation energy ECI's were then determined by adding the ECI's calculated in the respective cubic lattices. For $c/a$ ratios $\leqslant 1.2$ we minimized the error in the energy differences relative to the structures in the bcc lattice, while for $c/a$ ratios $>1.2$ the energy difference relative to the structure in the fcc lattice was used. This fitting procedure guarantees that, at $c/a=1$ and $c/a=\sqrt{2}$, the values of the ECI's comply with the symmetry requirements of the cubic lattice. A sixth-degree polynomial function was used for the $c/a$ dependence of the formation energy ECI's. This polynomial function provides a satisfactory fit to the energy curves for the pure transition metals deformed through the Bain path calculated in Ref. 1. For all symmetrically equivalent clusters, the slope of the ECI's functions relative to the $c/a$ ratio were constrained to add to zero at the points of cubic symmetry. This requirement was previously shown[20] to be also symmetry dictated and guarantees that all cubic structures, ordered or disordered, will display an energy extrema when deformed though a Bain distortion. Conversely, no particular functional form was assumed for the volume dependence. Each least-square fit was carried out at a constant volume of the bct lattice, and it was repeated for a range of volumes between the equilibrium

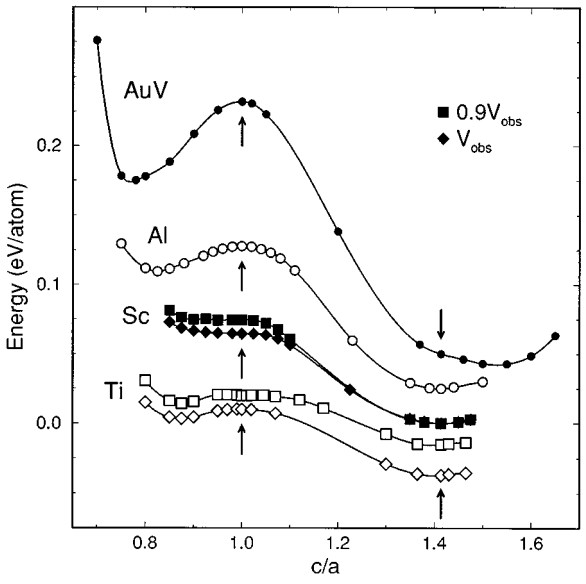


FIG. 2. Energies of Ti, Sc, Al, and AuV along the Bain distortion for the calculated fcc volume. For Ti and Sc, the energies ($\diamond$) for the observed volumes $V_{\rm obs}$ are also shown. Note that the curves have been displaced vertically for clarity.

volume of Ni and the equilibrium volume of Cr. The volume used for each fitting was determined by the weighted average of volumes of the pure components (Vegard's law) with an interval of composition of 0.05. Having the functions describing the $c/a$ dependence of the ECI's in a range of volumes between pure Ni and pure Cr, one can calculate with Eq. (1) the energy of the disordered bcc and fcc phases deformed through the Bain distortion path.

## III. RESULTS

### A. Bain distortion: Ordered systems

The Bain distortion for the transition metals series has been discussed previously.[1,12] Along this path, the crystal volume is constrained to be constant; implications associated with this are discussed in Appendix B. In Fig. 2, several examples demonstrating different aspects of the distortion energetics are shown.

First consider Ti whose high-temperature phase is bcc. The calculations for Ti give $T=0$ K volumes that are roughly 90% of the observed hcp volume. Such contractions are characteristic of LDA predictions, although they are much more severe for the $3d$ transition-metal elements and their compounds than they are for their $4d$ and $5d$ counterparts. There are extrema at both the bcc ($c/a=1$) and fcc ($c/a=\sqrt{2}$) structures. As a function of volume, the bcc extremum evolves from a maximum at large volumes to a shallow minimum at a volume of $\sim 0.9V_{\rm obs}$. This minimum by itself, however, is not enough to explain the stability of the high-temperature bcc phase: The well depth is comparable to or smaller than thermal vibrational energies and, more importantly, the thermal expansion of the lattice at the transition temperature ($\sim 3\%$) will cause the bcc phase to be a local maximum.

The distortion path has the general features that the energy must grow for both small and large values of $c/a$ and there must be one more minimum than maximum. Hence, if either the bcc or fcc structure is a maximum, another minimum must exist, but its position is not determined by symmetry. For Ti, this minimum occurs at $c/a\sim 0.85$. Elements do form in this compressed body-centered-tetragonal structure, the prototypes being Sn under pressure and protactinium.

Like Ti, Sc has its volume minimum at $\sim 0.9V_{\rm obs}$. However, in contrast to most of the transition metals, Sc (Fig. 2) has an inflection point at the bcc structure. Thus, bcc Sc is locally unstable without having a local maximum. (Sc remains hcp up to its melting point, in part because its melting temperature is lower than Ti and the bcc–fcc/hcp energy difference is larger.) From these and previous results, we have examples of transition metals which illustrate each of the various possibilities of maxima, minima, or inflection points at the high-energy phase, although maxima are the rule rather than the exception.

The cases considered up to now have involved transition metals. While there is no reason to expect that main group elements should behave differently, it is still desirable to see whether the high-energy phases are metastable or not. Both the fcc and bcc phases of Al have their energy minima at $\sim 0.96V_{\rm obs}$ and the distortion path has been taken at this volume. As seen in Fig. 2, the bcc has a local maximum with an accompanying minimum, while the low-temperature fcc phase is a minimum; the bcc–fcc energy difference is even larger than those of Ti and Sc. The overall behavior of Al is similar to the transition metals; in all cases where a distortion path has been followed through a low-temperature phase, an energy minimum has been observed.

AuV was chosen as an example of a compound which should have a $c/a$ ratio close to the ideal fcc value since this system forms as a disordered fcc alloy at this composition. The results in Fig. 2 show a local maximum for the CsCl ($c/a=1$) structure, which being cubic must have an extremum. No such condition holds for the ideal fcc-like CuAu-I ($c/a=\sqrt{2}$) whose atomic packing makes it intrinsically tetragonal; in fact, the minimum occurs at a slightly larger than ideal $c/a$ value. A small break in smoothness of the plot can be seen in the vicinity of this minimum. It is not an accident of the plotting or of the fitting scheme which lay a curve through the point. Instead it arises from an interplay of the reciprocal-lattice cutoff, the finite LASTO basis and $k$-point sets, and the varying $c/a$. An improvement in basis and $k$-point sets for this system would remove this feature.

### B. hcp to bcc path

To describe the hcp to bcc transition, we consider a different path. Both the bcc and hcp structures can be described by a based-centered orthorhombic two-atom unit cell described by the lattice constants $a$, $b$, and $c$. The atoms are at (0,0,0) and ($\xi a$,0,$c$/2). The relationship between the orthorhombic parameters and the conventional cells are: bcc structure, $a=c=\sqrt{2}a_{\rm bcc}$, $b=a_{\rm bcc}$, and $\xi=1/2$; hcp structure, $a=\sqrt{3}a_{\rm hcp}$, $b=a_{\rm hcp}$, $c=c_{\rm hcp}$, and $\xi=1/3$. The nearest and next-nearest neighbors in- ($d_1$, $d_2$, respectively) and out- ($d_3$, $d_4$, respectively) of plane are ($a>b$)

$$d_1^2=\frac{a^2}{4}+\frac{b^2}{4}, \tag{2a}$$

$$d_2^2=b^2, \tag{2b}$$

$$d_3^2=a^2\left(\xi-\frac{1}{2}\right)^2+\frac{b^2}{4}+\frac{c^2}{4}, \tag{2c}$$

$$d_4^2=a^2\xi^2+\frac{c^2}{4}. \tag{2d}$$

Let $d_1=d_3$ and $d_2=d_4$, i.e., (second) nearest-neighbor distances in and out of the plane be equal. If, in addition, the volume $\Omega=(1/2)abc$ remains constant, we obtain the following relationships:

$$\frac{c^2}{a^2}=4\xi(1-\xi), \tag{3a}$$

$$\frac{b^2}{a^2}=\xi, \tag{3b}$$

$$a^3=\frac{\Omega}{\xi(1-\xi)^{1/2}}. \tag{3c}$$

All the orthorhombic parameters are now given in terms of the single parameter $\xi$ corresponding to the in-plane position of the second atom in the basis. Moreover, at $\xi=1/3$ corresponding to hexagonal in-plane ordering,

$$\left(\frac{c}{a}\right)^2=\frac{8}{9}=\frac{1}{3}\left(\frac{c}{a}\right)^2_{\rm hcp}, \tag{4}$$

i.e., the ideal hcp $c/a$. Likewise, for $\xi=1/2$, Eqs. (3) give the correct bcc relationships. Thus the path from bcc to ideal hcp defined by Eqs. (3) maintains bond lengths while bond angles change. This path is a particular combination of a bcc $N$-point $T_1$ phonon (corresponding to changes in $\xi$ from the bcc position) and a long-wavelength shear.

The transition metals which form in the hcp structure have $c/a$ ratios which are measurably smaller than the ideal value of $\sqrt{8/3}$. The bcc metals, however, have their energy minima for the hcp at $c/a$ which are larger, as seen for Mo and Nb in Fig. 3. While hcp Nb is lower in energy than fcc Nb, consistent with Kaufman's[7] assumptions, Mo has [as do W and Ta (Ref. 11)] the fcc structure lying lower. This reversal of the hcp–fcc energy differences has adverse consequences for those types[7] of phase diagram constructs.

In Fig. 4 the energies along the bcc–hcp path are shown for Mo and Nb. The total energies have extrema at both the bcc and hcp positions. However, as seen in Fig. 3, neither hcp Mo nor hcp Nb have $c/a$ ratios close to ideal. For nonideal hcp $c/a$ values, the relationships given in Eqs. (3) no longer hold and must be modified. There are many possible ways to alter the path (corresponding to different mixtures of the $T_1$ phonon and the shear) between the hcp and bcc structures, but not all will have extrema in the energy at the endpoints. As discussed in Appendix A, there are certain symmetry-dictated conditions that will guarantee that there will be extrema; the ideal $c/a$ path satisfies these conditions and the modification for nonideal $c/a$ given in Eq. (A9) also

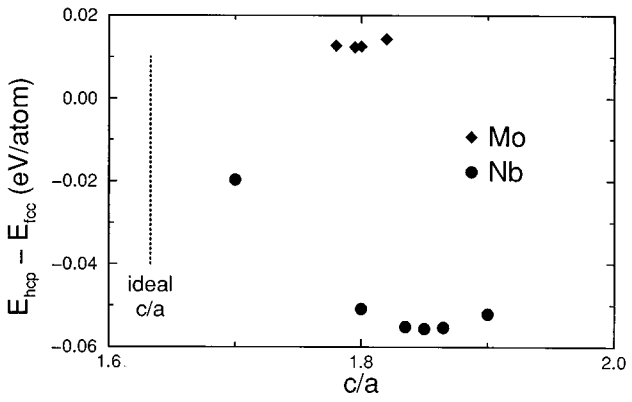


FIG. 3. Calculated total energy difference between the hcp and fcc structures as a function of $c/a$ for Mo and Nb. The ideal $c/a$ value of $\sqrt{8/3}$ is given for comparison.

does. If, however, the path is modified slightly so that the conditions are no longer satisfied, the energy will not have an extremum (Path $B$ of the inset to Fig. 4), pointing out the obvious point that the energy at the nonequilibrium phase is a saddle point.

### C. PtTi and PtV

PtTi and PtV form in the orthorhombic AuCd structure at low temperatures and undergo Martensitic transitions at ~1300 and 1773 K to the CsCl and CuAu-I structures, re-

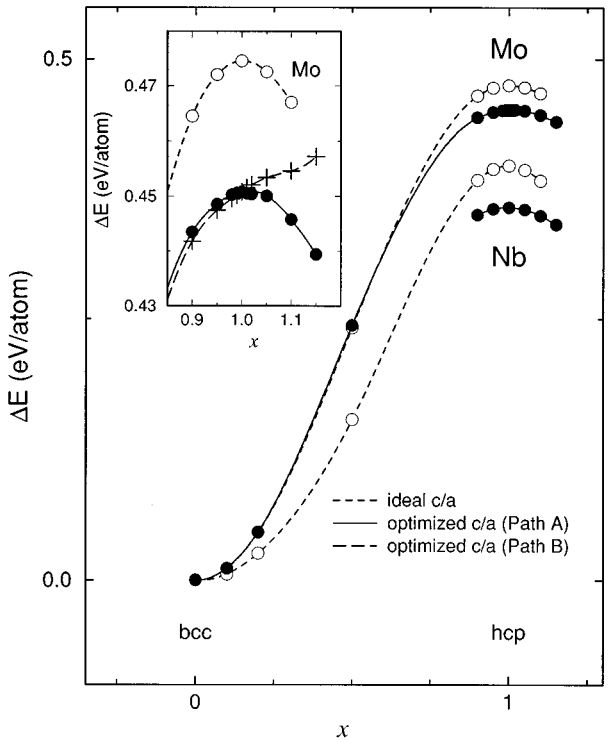


FIG. 4. Total energy along the bcc to hcp path for Mo and Nb. For ideal $c/a$ ratio, the path is defined by Eq. (3). For the calculated hcp $c/a$ ratio, Path $A$, described in Appendix A, is followed. In the inset, the region around the hcp structure for Mo is shown, including a path (Path $B$) similar to Path $A$ that does not satisfy $\delta c/\delta x|_{x=1}=0$ $(x=3-6\xi)$.

spectively. The reported[22] crystallographic data for the CsCl structure indicates a larger volume per molecular unit than for the low-temperature phase as is to be expected. The reverse is reported for PtV CuAu-I, which seems unlikely. Nevertheless, the reported $c/a$ for the CuAu-I structure and the reported $c/a$ and $b/a$ for the AuCd were employed and lattice volumes were varied to determine the LDA energy minima. (This choice was made because LDA calculations usually yield $c/a$ close to experiment with total energies close to those calculated for the observed $c/a$ and not searching for these ratios represented significant savings in computer time.) The $T=0$ volumes of the high- and low-temperature phases were found to be almost identical and corresponded to $0.986V_{\text{obs}}$(AuCd) for PtTi and 0.955 $V_{\text{obs}}$(AuCd) for PtV. The AuCd structure has an internal parameter corresponding to adjacent lines of atoms parallel to the $c$ axis sliding with respect to each other. With the position of one line defined by the fraction $x$ of the unit cell's $c$ value, $x=0.25$ corresponds to the regular spacing of the CsCl and CuAu-I structures. The internal coordinates of the AuCd structure were not reported in the crystallographic data for either PtTi or PtV; the calculated values for these compounds are 0.19 and 0.176, respectively. Given the lattice parameters a simple distortion path interpolating between the phases was chosen:

$$a=a(LT)-\Delta[a(LT)-a(HT)], \tag{5a}$$

$$b=b(LT)-\Delta[b(LT)-b(HT)], \tag{5b}$$

$$c=c(LT)-\Delta[c(LT)-c(HT)], \tag{5c}$$

$$x=0.25-\Delta[0.25-x(HT)], \tag{5d}$$

where $a$, $b$, and $c$ are the lattice constants of the low, $LT$, and high, $HT$, temperature phases. The energies, as a function of $\Delta$, appear in Fig. 5. (For PtV, results for one intermediate value of $\Delta$ is shown to indicate the height of the barrier between the two phases.) The high-temperature phases are seen to have energy extrema for the chosen distortion path: PtTi is a local maximum, as has usually been the case, while PtV is a minimum which is unusual and likely is associated with the calculated near degeneracy of the two phases. The AuCd phases show minima whose positions are not controlled by symmetry considerations. The chosen distortion path, Eqs. (5), constrains the $b/a$ and $c/a$ to particular combinations and they are such that the calculated minimum occurs at a $\Delta$ somewhat larger than one for PtTi. (These paths do not have symmetry-dictated extrema at $\Delta=0$ or 1.) For PtV, the high-temperature phase is calculated to have a slightly lower energy than the low-temperature AuCd structure. Suffice it to say, the important feature of these results is that a compound having a high-temperature Martensitic phase is calculated to be unstable to local distortions, while another compound is found to be locally stable.

### D. Ni-Cr system

As described in Sec. II, the energy of the disordered Ni-Cr alloys was determined using the cluster expansion method. The three first pair interactions in the tetragonal lattice (out of seven used in the expansion) are plotted as a function of $c/a$ ratio in Fig. 6. The pair interactions are plotted for a fixed volume given by Vegard's law, at a composition of 0.5 Cr. Figure 6 shows that the first-neighbor ECI changes sign when the $c/a$ ratio changes from 1 to $\sqrt{2}$. The negative value of the ECI in the bcc lattice suggests that the system in this lattice will tend to segregate, while the positive value in the fcc lattice suggests that in this lattice, the system will tend to order. This change in the sign of the ECI is reflected in the NiCr phase diagram. In the Cr-rich side of the phase diagram, where the bcc lattice is more stable, there is a tendency

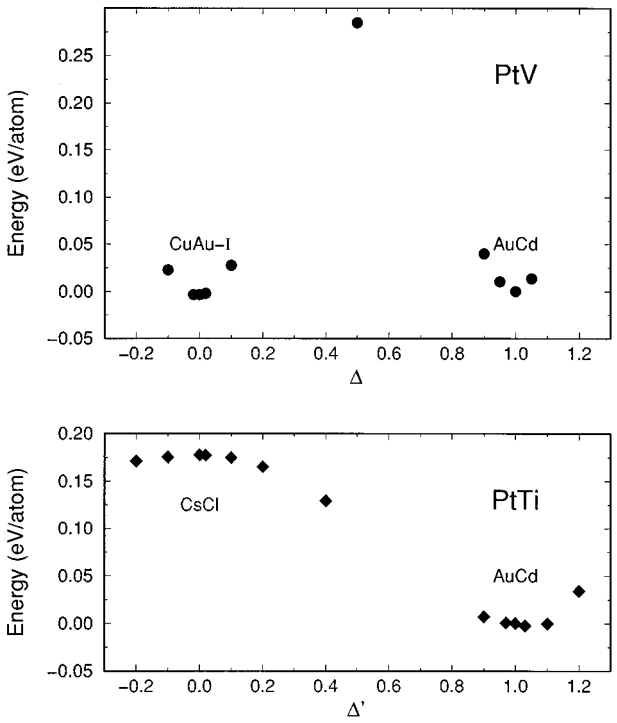


FIG. 5. Total energies, relative to the low-temperature AuCd phases, for PtTi and PtV along the distortion paths defined by Eq. (5).

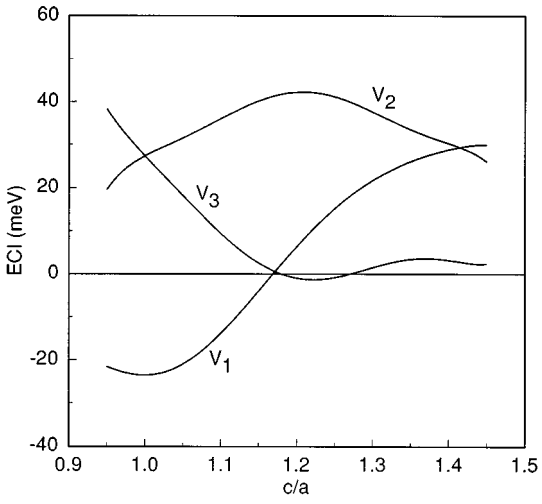


FIG. 6. First ($V_1$) to third ($V_3$) pairs ECI's plotted as a function of $c/a$ ratio for the Ni-Cr system. The ECI's are plotted at constant volume for a composition of 50% Cr.

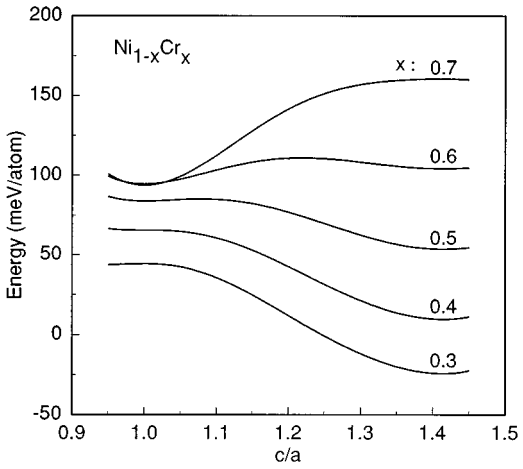


FIG. 7. Formation energy of disordered Ni-Cr alloys along a constant volume Bain distortion path for various concentrations of Cr.

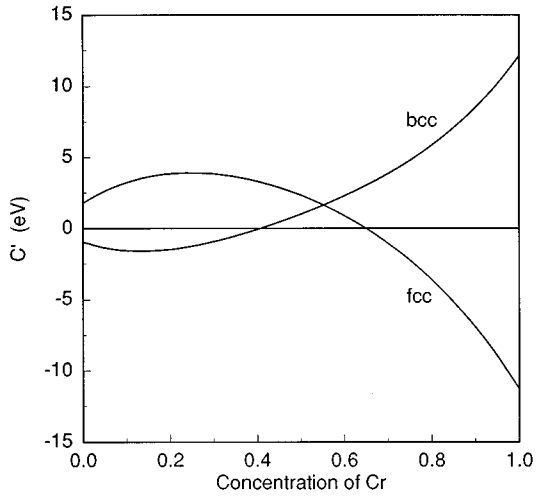


FIG. 8. Shear constants $C'=(c_{11}-c_{12})/2$ plotted as a function of composition for the fcc and bcc phases in the Ni-Cr system.

for segregation. Conversely, in the Ni-rich side, where the fcc lattice is more stable, the Ni-Cr system orders in a $MoPt_2$ prototype structure.[10]

In addition to showing the change in sign of the first-neighbor ECI, Fig. 6 exemplifies the splitting of some clusters when the symmetry of the lattice is broken. At $c/a=1$ the set of first-neighbor pairs in the tetragonal lattice is also the set of first-neighbor pairs in the bcc lattice and do not split as the $c/a$ ratio deviates from 1. At $c/a=\sqrt{2}$, the set of first-neighbor pairs in the bct lattice comprise eight of the fcc's first neighbors. The remaining first neighbors in the fcc lattice come from the set of second-neighbor pairs in the bct lattice. A similar splitting of sets of clusters occurs with the second pair in the bcc lattice, also shown in Fig. 6. When passing from a cubic to a tetragonal lattice, the splitting of sets of clusters will occur every time one set in the bcc lattice is related by the distortion to more than one set in the fcc lattice or vice versa. Figure 1 gives the relation between the clusters used in the bcc and fcc lattices.

The energy of the disordered $Ni_{1-x}Cr_x$ alloy deformed through a Bain distortion is plotted in Fig. 7 for a range of composition $x=0.3$ to 0.7. Each curve is drawn at constant volume determined by Vegard's law. Figure 7 shows the transition in mechanical stability of the bcc and fcc phases. At 30% Cr, the fcc phase lies in a local minimum in energy, while the bcc phase has a local maximum, similar to pure Ni. As the concentration of Cr increases, there is a composition range where both the bcc and fcc phases are at a local minima in energy, thus being mechanically stable to this deformation mode. As the concentration of Cr increases further, the bcc phase remains at a minimum but the fcc phase becomes unstable, similar to the behavior of pure Cr.

A quantitative analysis of the mechanical stability of the disordered bcc and fcc structures can be obtained from the calculation of the elastic constants $C'=(c_{11}-c_{12})/2$. For the Bain distortion path at constant volume, the curvature of the energy function at $c/a=1$ and at $c/a=\sqrt{2}$ are proportional to the $C'$ shear constants of the bcc and fcc phases. These elastic constants are plotted in Fig. 8. The region of mechanical stability of each phase is given by the sign of the shear constant. Figure 8 shows that at 0 K only the fcc phase is stable for concentrations lower than 41% Cr. As the concentration of Cr increases, the bcc phase becomes mechanically stable. Both phases are stable up to a concentration of 65% Cr. For concentrations higher than 65% Cr, the bcc phase is mechanically stable to this deformation mode, while the fcc phase is unstable. As discussed in the Introduction, some semiempirical methods to construct phase diagrams implicitly assume that the nonequilibrium phase is metastable, which guarantees that the free energy of the phase is defined throughout the whole composition range. Clearly the assumption of metastability for the nonequilibrium phases is not fulfilled for the whole composition range.

A further result that can be obtained from our calculation is the relationship between energy difference of the cubic phases and the $C'$ shear constants. Wills *et al.*[3] observed that for the pure elements in the 3*d* transition-metal series, the $C'$ shear constant of the lower energy phase is approximately proportional to the energy difference between the bcc and fcc phases. Although this observation may apply to the pure elements, our results show that it does not apply for disordered compounds in the Ni-Cr system. At a concentration of $\sim$57% Cr, the fcc and bcc phases have the same energy. According to the assumption of Wills *et al.*, at this concentration the second derivative of the energy with respect to $c/a$ ratio of either phases should be zero. Figure 8 shows that at 57% Cr, both structures have a $C'$ shear constant different from zero.

A better correlation between the $C'$ and the energy difference between the bcc and fcc phases can be determined from the symmetry-dictated conditions on the topology of the energy curve of a disordered system. For the Bain distortion path at a constant volume, the first derivative of the energy relative to $c/a$ must vanish at $c/a=1$ and $c/a=\sqrt{2}$. Assuming a fourth degree polynomial for the $c/a$ ratio dependence of the energy, the zero slope constrain implies that $E_{\mathrm{fcc}}-E_{\mathrm{bcc}}\propto 1/2C'_{\mathrm{fcc}}-C'_{\mathrm{bcc}}$. Although this relation is not valid for higher-order polynomials, it suggests that the energy difference between the cubic phases can be correlated to a difference in the $C'$ shear constants of the bcc and fcc phases. The difference in the $C'$ shear constant plotted as a function of the energy difference between the bcc and fcc phases is

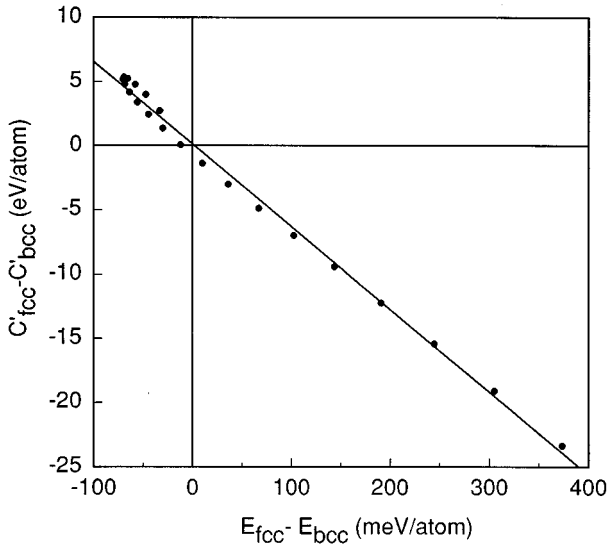


FIG. 9. Correlation between the difference in bcc and fcc shear constants, $C'_{\rm fcc}-C'_{\rm bcc}$ and energy differences, $E_{\rm fcc}-E_{\rm bcc}$, for the disordered Ni-Cr system at different concentrations.

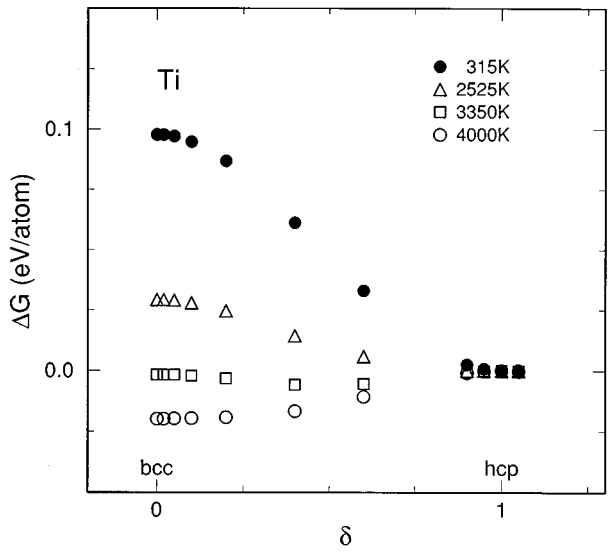


FIG. 10. Gibbs energy $\Delta G(P=0)$, including electronic entropy contributions, for Ti along the hcp-bcc path at various temperatures. Energies are given relative to the hcp phase at each temperature.

shown in Fig. 9. The plot is shown for the whole range of composition with an increment of 0.05 between each point. As shown in the plot, a good correlation is found between the two quantities. Also plotted in Fig. 9 is a linear fit to the $C'$ shear constant difference as a function of the energy difference between the cubic phases.

## IV. FINITE-TEMPERATURE EFFECTS

As discussed briefly previously, a number of elements and compounds are experimentally found to have a structural phase transition at high temperature, even though the high-temperature phase is mechanically unstable at $T=0$. Although the expansion of the lattice with temperature will affect the energies, the local stability of these high-temperature phases still must be due in large part to entropy contributions, both electronic and vibrational, to the free energy.[1] While vibrational contributions are generally considered to be more important,[23,24] differences in the electronic contributions between different phases have been shown[25] to be of the same magnitude as the entropy changes inferred from experiments. Conceptually, the simplest model of these phase transitions is the soft-mode picture. For Ti, however, there is strong experimental evidence[26] that this simple picture is not applicable, even though there are low-energy phonons in the high-temperature bcc phase. Another class of models, which does not require soft modes, attributes these Martensitic transformations to fluctuations related to anharmonicities.[27–30]

Recently a number of different approaches have coupled first-principles electronic structure calculations with other models such as anharmonic phonon perturbation theory[31] and Landau-Ginzburg models[32] to investigate these phase transitions. In addition, direct calculation of the entropy contributions to the free energy has also been attempted.[9] While progress has been made, none of these models are yet able to predict the transition temperatures from first principles. The major difficulty in all these studies is in determining the contribution of the vibrational entropy to the free energy, especially when phases are mechanically unstable.

In this section, we will present results for Ti along the hcp–bcc distortion path at finite *electronic* temperature, thus including the electronic entropy, but ignoring the vibrational entropy. Even in this drastic approximation there are notable effects with temperature. A simple example is the lattice expansion (because of the filling of more antibondinglike states): the lattice expands, but the coefficient of linear thermal expansion is about an order of magnitude smaller than the experimentally observed one, as one would expect. More important for this paper and questions of mechanical stability are how the energy differences between different phases change.

The results of the electronic entropy for Ti at various temperatures are shown in Fig. 10. As the temperature is increased, the difference between the bcc and hcp phases decreases, i.e., the electronic entropy stabilizes the bcc phase. At an electron temperature of $\sim$2525 K, the hcp phase is no longer a local minimum, and *both* the bcc and hcp phases are mechanically unstable. Not until temperatures of around 3350 K does the bcc phase become lower in energy than the hcp, but the minimum occurs for a $\delta$ between the hcp and bcc structures. Finally, at an electron temperature of around 4000 K the bcc phase becomes both mechanically stable and lowest in energy. Thus, for Ti at least, thermal electronic excitations are enough to cause a phase transition, albeit at extremely high (above the melting point) temperatures.

Our value of 3350 K for the electron temperature where the bcc is lower in energy than the hcp phase is significantly larger than found (2050 K) by Moroni *et al.*[9] This difference, however, is simply related to the fact that we find a larger hcp–bcc energy difference (99 meV/atom versus 62 meV/atom[9]); almost perfect agreement is obtained by simply scaling the temperatures by the hcp–bcc energy differences. The discrepancy between the calculations most likely results from Moroni *et al.*'s use of the atomic-sphere approximation,

instead of a full potential method such as used here. (Full-potential LMTO calculations[33] give 0.09 eV/atom, in reasonably good agreement with our results.)

The phase transition is experimentally determined to occur at 1153 K, rather than the 4000 K expected if only electronic effects are considered. Thus, vibrational, particularly anharmonic, contributions to the free energy must be significant. While a detailed modeling of the hcp–bcc transition is beyond the scope of this paper, several observations can be made: (i) The scale of the energies shown in Fig. 10 is the same as $k_B T$ at the transition temperature. (ii) At the observed transition temperature, the bcc phase is still mechanically unstable, but both the hcp–bcc energy difference is smaller and $(\hbar\omega)^2$ of the unstable bcc $N$-point $T_1$ phonon decreases in magnitude by $\sim 20\%$. (iii) The electronic contributions to the entropy are important, but only provide about 1/3 of the entropy required at the experimental transition temperature, consistent with the estimate of 70% for the vibrational contributions inferred from experiment[26] and estimates made previously.[25] This observation, however, is contrary to that of Moroni *et al.*[9] who conclude from their approximate calculations of the vibrational entropy that the electronic energies are the major driving force of the hcp–bcc transition. Note that combining their estimates of $\Delta G_{\rm vib}$ with the more accurate full-potential hcp–bcc energy differences implies a calculated transition temperature for Ti that is far too large (by a factor of 2–3). This discrepancy requires further investigation, particularly whether important contributions to the vibrational entropy have been neglected. (iv) As is obvious from Fig. 10, the potential describing Ti is temperature dependent on a scale comparable to the temperature itself. The models[28,30] used to describe entropy-driven phase transitions will need to be extended to include this temperature dependence also.

## V. CONCLUSIONS

Although perhaps surprising, structural instabilities of excited (nonequilibrium) phases appear to be ubiquitous. As discussed previously,[1] these instabilities have important consequences for the modeling of phase diagrams and the interpretation of the parameters in those constructs. In this paper, we have extended the previous study[1] both to different systems and to different distortion paths. As for the Bain distortion, symmetry-dictated extrema of the energy exist for properly chosen paths connecting different high-symmetry structures. The systems considered in this paper illustrate the different behaviors possible and clarify the nature of the symmetry arguments.

An important advance has been made in determining the elastic constants (mechanical stability) of disordered alloys by using a cluster expansion appropriate to the tetragonal lattice. The $C'$ elastic constants were calculated for both the bcc and fcc phases along the Bain path for the disordered Ni-Cr system. Our results show there are concentration ranges where the cubic phases are mechanically unstable and the free energy at 0 K is not defined. As in the case of Ti, or PtTi in the CsCl structure, entropy will play an important role in mechanically stabilizing a phase in the alloy; at higher temperatures, the range of mechanical instability calculated may change when vibrational modes are included.

In this paper, we have addressed a number of apparently independent issues, but which are all related to the question of the mechanical stability of excited phases. Although not every system will show such instabilities, the possibility should not be excluded. While we have presented arguments of where instabilities might occur and given specific examples, the stability of an excited phase ultimately depends on the specifics of the system. Furthermore, the experimental observation of, for example, a high-temperature phase or a disordered alloy at some concentration, does not mean that these systems are mechanically stable at different temperatures or compositions. Models of phase diagrams that ignore these issues may well generate good interpolation schemes, but the underlying microscopic basis will need to be reexamined. Finally, the results presented in this paper demonstrate that microscopic electronic structure calculations can directly address macroscopic questions such as the mechanical stability of alloy phases.

## ACKNOWLEDGMENTS

The work at Brookhaven was supported by the Division of Materials Sciences, U.S. Department of Energy, under Contract No. DE-AC02-76CH00016 and by a grant of computer time at the National Energy Research Supercomputer Center. The work at the University of Texas at Austin was supported by the National Science Foundation under Grant No. DMR-91-14646. P.J.C. wishes to acknowledge CNPq (Brazil) for their financial support.

## APPENDIX A: SYMMETRY-DICTATED EXTREMA

As in the case of the fcc to bcc Bain distortion, the bcc to hcp path will have symmetry-dictated zero derivatives (extrema) in the total energy if certain conditions are met. Let $x=3-6\xi$ be a measure of the distortion along the bcc $(x=0)$ to hcp $(x=1)$ path. As defined in Sec. III B, $\xi$ is a measure of the atomic position along the $a$ axis of one of the two atoms in the base-centered-orthorhombic cell. If the distortion is at constant volume, then

$$\frac{\delta a}{a}+\frac{\delta b}{b}+\frac{\delta c}{c}=0. \tag{A1}$$

The single independent parameter defining the path (and the lattice parameters $a$, $b$, and $c$) is $x$. For the energy, or similar type function, given by $U=U(a,b,c;x)$, the change in energy due to variations in the parameters is

$$\delta U=\left(\frac{\delta U}{\delta a}\frac{\delta a}{\delta x}+\frac{\delta U}{\delta b}\frac{\delta b}{\delta x}+\frac{\delta U}{\delta c}\frac{\delta c}{\delta x}\right)\delta x. \tag{A2}$$

Using Eq. (A1) to eliminate $\delta b$ results in

$$\frac{\delta U}{\delta x}=\left(\frac{\delta U}{\delta a}-\frac{b}{a}\frac{\delta U}{\delta b}\right)\frac{\delta a}{\delta x}+\left(\frac{\delta U}{\delta c}-\frac{b}{c}\frac{\delta U}{\delta b}\right)\frac{\delta c}{\delta x}. \tag{A3}$$

For the bcc structure, we have $a=c$ and $a=\sqrt{2}b$. These relationships, and the related ones among the derivatives, e.g., $\delta U/\delta a=\delta U/(\sqrt{2}b)$, cause the terms in both sets of parentheses to vanish; hence,

$$\left.\frac{\delta U}{\delta x}\right|_{x=0}=0 \tag{A4}$$

and the energy will be an extremum along this path.

Around the hcp structure, $x=1$, $a$ and $b$ are related by

$$\frac{\delta U}{\delta b}=\sqrt{3}\frac{\delta U}{\delta a}. \tag{A5}$$

Combining these results, we have that Eq. (A3) becomes

$$\left.\frac{\delta U}{\delta x}\right|_{x=1}=\frac{\delta U}{\delta a}\left(1+\sqrt{3}\frac{\delta b}{\delta a}\right)\frac{\delta a}{\delta x}+\frac{\delta U}{\delta c}\frac{\delta c}{\delta x}. \tag{A6}$$

In general, there is no simple relationship between $\delta U/\delta c$ and $\delta U/\delta a$. To ensure an extremum, we *require*

$$\left.\frac{\delta c}{\delta x}\right|_{x=1}=0. \tag{A7}$$

This condition plus volume conservation, Eq. (A1), gives

$$\left.\frac{\delta b}{\delta a}\right|_{x=1}=-\frac{b}{a}=-\frac{1}{\sqrt{3}}. \tag{A8}$$

Combining these results yields $\delta U/\delta x|_{x=1}=0$. Thus, the conditions necessary to guarantee an extremum at the hcp structure are Eq. (A1) (volume conservation) and Eq. (A7) (first-order variations in $c$ with respect to $x$ to vanish).

The path between the bcc and ideal hcp structures defined by Eqs. (3) satisfies these conditions, thus explaining the extremal behavior observed in Fig. 4 for ideal $c/a$. For non-ideal $(c/a)_{\rm hcp}$, a simple modification of Eq. (3a) that satisfies these conditions around $x=1$ is

$$\left(\frac{c}{a}\right)^2=\frac{3}{8}\left(\frac{c}{a}\right)^2_{\rm hcp}\left(1-\frac{x^2}{9}\right). \tag{A9}$$

While this form cannot be used over the whole path since it does not include the bcc structure, a path that (for example, quadratically) interpolates between Eqs. (3a) and (A9) will satisfy the conditions at both endpoints. The solid curves of Fig. 4 follow this path around the hcp structure while Path $B$ in the figure for Mo shows the effect when a small $\delta c/\delta x\neq 0$ contribution exists, thereby violating the symmetry conditions described above.

## APPENDIX B: GIBBS vs HELMHOLTZ FREE ENERGIES

At a phase transition, it is normally Gibbs free energies $G$ that must be compared. Most of the results in this paper, on the other hand, have presented the internal energy $E$ at constant volume. At $T=0$, $E$ is equivalent to the Helmholtz free energy and is related to the Gibbs energy by

$$G=E+PV, \tag{B1}$$

where $P$ is the pressure and $V$ is the volume. A naive—and unfortunately rather common—interpretation of Eq. (B1) suggests that that an additional term $PV$ should be added to the internal energy if the volume changes along the path. These effects are not small: For Ir, the difference between the fcc and bcc volumes is $\sim 3.5\%$ and the pressure needed to compress the bcc phase to the fcc volume is $\sim 100$ kbars, implying $PV\approx 1$ eV/atom. Such an enormous additional energy term would significantly alter conclusions regarding the relative stability of different phases.

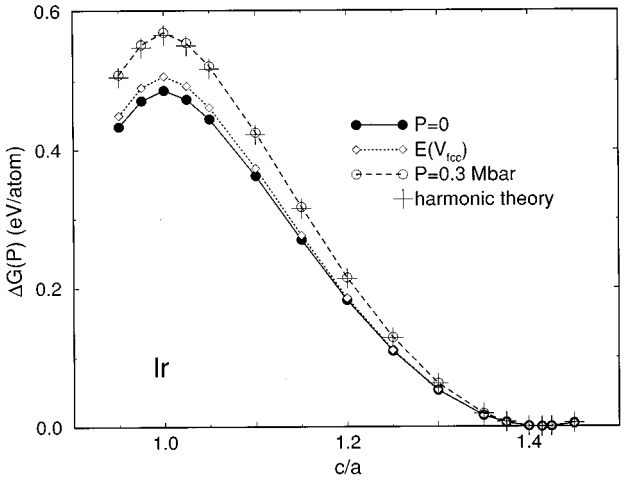


FIG. 11. Gibbs energy $G(P)$, $P=0$, 0.3 Mbar, and $E(V_{\rm fcc})$ (relative to the fcc values) for Ir along the Bain distortion calculated using the LMTO-ASA.

The resolution of this apparent problem is straightforward. In thermodynamics the independent variables determine which potential to consider: While the Gibbs energy is the correct thermodynmaical potential at *constant pressure*, the Helmholtz free energy (which is simply $E$ at $T=0$) should be used at constant volume.[34] While $E(V)+PV$ at constant *volume* looks like a Gibbs energy, the independent variable is $V$, not $P$, and thus is *not* thermodynamically meaningful.

Clearly $G(P)$ and $E(V)$ do differ since $V$ may vary for different values of $c/a$ along the Bain path. As an example, the calculated values[35] of $\Delta G(P)$ for Ir at $P=0$ and 300 kbars are given in Fig. 11, along with the energy at constant volume. The relative difference in energy between the Helmholtz energy at $V_{\rm fcc}$ and the Gibbs energy at $P=0$ is $\sim 0.02$ eV/atom. Even for large pressures, the overall shape and magnitude are quite similar.

These results are easy to understand: For a given phase, let $\Omega$ be the reference volume, $V_0$ the volume at $P=0$, and $B$ the bulk modulus. Then, within harmonic theory,

$$G(P)=E(\Omega)+P\Omega-\frac{1}{2}B\Omega\left(\frac{\Omega}{V_0}\right)\left[\frac{V_0}{\Omega}\left(1-\frac{P}{B}\right)-1\right]^2. \tag{B2}$$

Although the $P\Omega$ term may be large, it is a constant for any $P$. Differences between the last term of Eq. (B2) for different phases are typically $\sim 0.01$–$0.10$ eV/atom, depending on $P$. (For systems in which the overall energy scale is smaller, this contribution is also proportionally smaller.) Relative changes between phases (e.g., fcc and bcc) with respect to $P$ are due to variations in $B$ and/or $V_0$. As shown in Fig. 11, this simple harmonic theory reproduces the results of the full calculations quite well. Thus, the differences between $G(P)$ and $E(V)$, while formally important when considering constant $P$ phase transitions, are relatively small in magnitude and will not alter the general trends.

[1] P. J. Craievich, M. Weinert, J. M. Sanchez, and R. E. Watson, Phys. Rev. Lett. **72**, 3076 (1994).
[2] G. W. Fernando, J. Mei, R. E. Watson, M. Weinert, and J. W. Davenport, Phys. Rev. B **47**, 13 636 (1993).
[3] J. M. Wills, O. Eriksson, P. Söderlind, and A. M. Boring, Phys. Rev. Lett. **68**, 2802 (1992); P. Söderlind, O. Eriksson, J. M. Wills, and A. M. Boring, Phys. Rev. B **48**, 5844 (1993).
[4] T. Kraft, P. M. Marcus, M. Methfessel, and M. Scheffler, Phys. Rev. B **48**, 5886 (1993).
[5] A. Y. Liu and D. J. Singh, Phys. Rev. B **47**, 2757 (1993).
[6] S. Peng and H. J. F. Jansen, J. Appl. Phys. **67**, 4567 (1990).
[7] L. Kaufman and H. Bernstein, *Computer Calculations of Phase Diagrams* (Academic, New York, 1970); also see the journal CALPHAD.
[8] A. Fernández Guillermet, V. Ozoliņš, G. Grimvall, and M. Körling, Phys. Rev. B **51**, 10 364 (1995).
[9] E. G. Moroni, G. Grimvall, and T. Jarlborg, Phys. Rev. Lett. **76**, 2758 (1996).
[10] J. Murray, L. H. Bennett, and H. Barker, *Binary Alloy Phase Diagrams* (American Society for Metals, Metals Park, OH, 1986).
[11] G. W. Fernando, R. E. Watson, M. Weinert, Y. J. Wang, and J. W. Davenport, Phys. Rev. B **41**, 11 813 (1990).
[12] A. Chang, C. Colinet, M. Hillert, Z. Moser, J. M. Sanchez, N. Saunders, R. E. Watson, and A. Kussmaul, CALPHAD **19**, 481 (1995).
[13] G. W. Fernando, J. W. Davenport, R. E. Watson, and M. Weinert, Phys. Rev. B **40**, 2757 (1989).
[14] E. Wimmer, H. Krakauer, M. Weinert, and A. J. Freeman, Phys. Rev. B **24**, 864 (1981).
[15] Li is bcc at high temperatures and is observed to be fcc at intermediate temperatures upon heating the material from low temperatures. The energy difference between these phases is very small and calculations involving several thousand $k$ points failed to accurately establish the energy dependence of the Bain distortion path through the bcc structure. Accurate results would require either interpolation into $k$ space between the mesh of $k$ points or going to meshes of several tens of thousands of special $k$ points. This was not done. The results which were obtained however do suggest that the energy of bcc Li is unstable to local distortions.
[16] H. L. Skriver, *The LMTO Method* (Springer-Verlag, Berlin, 1984).
[17] J. M. Sanchez, F. Ducastelle, and D. Gratias, Physica **128A**, 334 (1984).
[18] J. M. Sanchez, Phys. Rev. B **48**, 14 013 (1993).
[19] P. E. A. Turchi, Mater. Sci. Eng. A **127**, 145 (1990).
[20] P. J. Craievich and J. M. Sanchez, in *Mechanical Stability in the Nickel-Chromium System*, Proceedings of the Workshop on Modelling and Simulation for Materials Design, edited by S. Nishijima and H. Onodera (Tsukuba, Japan, 1996), pp. 108–113.
[21] J. W. D. Connolly and A. R. Williams, Phys. Rev. B **27**, 5169 (1983).
[22] P. Villars and L. D. Calvert, *Pearson's Handbook of Crystallographic Data for Intermetallic Phases* (American Society for Metals, Metals Park, OH, 1991).
[23] C. Zener, Phys. Rev. **71**, 846 (1947).
[24] J. Friedel, J. Phys. (Paris) Lett. **35**, L59 (1974).
[25] R. E. Watson and M. Weinert, Phys. Rev. B **30**, 1641 (1984).
[26] W. Petry, A. Heiming, J. Trampenau, M. Alba, C. Herzig, H. R. Schober, and G. Vogel, Phys. Rev. B **43**, 10 933 (1991).
[27] P. C. Clapp, Phys. Status Solidi B **57**, 561 (1973).
[28] J. A. Krumhansl and R. J. Gooding, Phys. Rev. B **39**, 3047 (1989); J. A. Krumhansl, Solid State Commun. **48**, 251 (1992).
[29] P. Lindgård and O. G. Mouritsen, Phys. Rev. Lett. **57**, 2458 (1986).
[30] W. C. Kerr and M. J. Rave, Phys. Rev. B **48**, 16 234 (1993).
[31] Y.-Y. Ye, Y. Chen, K.-M. Ho, B. N. Harmon, and P. Lindgård, Phys. Rev. Lett. **58**, 1769 (1987).
[32] K. Schwarz, P. Mohn, V. L. Sliwko, and P. Blaha, J. Phys. (Paris) Colloq. **56**, C2-47 (1995); P. Mohn, K. Schwarz, and P. Blaha, J. Phys. Condens. Matter **8**, 817 (1996).
[33] A. T. Paxton, M. Methfessel, and H. M. Polatoglou, Phys. Rev. B **41**, 8127 (1990).
[34] E.g., K. Huang, *Statistical Mechanics* (Wiley, New York, 1963), pp. 23–26.
[35] The calculations shown were done using the LMTO-ASA; FLASTO calculations give similar results for the differences between $\Delta G$ and $\Delta E$ (and lead to similar conclusions) even though the full-potential bcc-fcc energy difference is $\sim 0.2$ eV/atom larger.